

## ELASTIC PROPERTIES AND CRYSTALLIZATION OF THERMAL BARRIER COATINGS OF Cr<sub>2</sub>AlC

O. CRISAN\*, A. D. CRISAN

*National Institute for Materials Physics, PO Box MG-7, 077125 Bucharest, Romania*

The elastic and structural properties of thermal barrier coatings of Cr<sub>2</sub>AlC DC sputtered from elemental targets onto Si(100) substrate at 200°C are studied. The material was subsequently submitted to re-crystallization procedure by annealing the film at 650°C and 700°C in high vacuum and in air for 30 min. As-deposited and annealed films are shown to be homogeneous and dense over large areas. The re-crystallization process was monitored using X-ray diffraction and Raman spectroscopy. As-deposited films have an amorphous-like Cr-C-Al solid solution structure and annealed samples crystallize into single-phase hexagonal Cr<sub>2</sub>AlC. While XRD analysis and Raman spectroscopy of samples annealed in-air show the presence of 5% Cr<sub>2</sub>O<sub>3</sub>, the high vacuum samples annealed at 650°C and 700°C are fully crystallized and comprise only single-phase Cr<sub>2</sub>AlC hexagonal structure. Oxygen presence in the in-air annealed sample is shown to cause an elongation of the hexagonal unit cell along the c axis which coincides with the direction of stacking of Cr<sub>6</sub>C octahedral building blocks with alternate Al layers. Whereas the average grain size is shown to increase upon annealing, lattice microstrain, calculated using the integral breadth method, is seen to decrease by almost 70% in the annealed films. Raman spectra of as-deposited films show characteristic MAX-phase bands with broad, overlapping peaks in the region of 120-400 cm<sup>-1</sup> but also peaks in the range of 550-900 cm<sup>-1</sup>, attributed to other Raman-active modes of the Cr<sub>2</sub>AlC structure. After annealing, the Raman peaks corresponding to Cr<sub>2</sub>AlC single-phase are narrower, more intense and better defined than in the as-deposited case. The occurrence of the disorder-induced D carbon band is observed in the Raman spectrum of the as-deposited film while, after high vacuum annealing, a sharp and relatively intense peak attributed to the carbon G band is observed that suggests that there may be carbon nanoclustering in the coatings upon annealing. This observation is consistent with and comes as a confirmation of previously reported *ab initio* modelling of possible Cr<sub>2</sub>AlC off-stoichiometric structures.

(Received September 4, 2017; Accepted November 29, 2017)

*Keywords:* Ternary carbides, Thermal barrier coatings, Annealing, Crystallization

### 1. Introduction

The ternary compounds known as MAX phases, where M is a transition metal, A is a metalloid, or more generally, a group III A or IV A element and X is either C or N, have attracted very large interest since it has been discovered that they exhibit both metallic and ceramic features. Although discovered in the 1960's by Jeitschko and Novotny [1], the larger class of alloys M<sub>n+1</sub>AX<sub>n</sub> where n = 1, 2 or 3, has lately attracted extremely large scientific interest since Barsoum and El-Raghy [2] synthesized single-phase bulk Ti<sub>3</sub>SiC<sub>2</sub> and found it to exhibit high electric and thermal conductivity, to be easy machinable, extremely stiff and highly resistant to oxidation and thermal shocks. In the form of thin films, these alloys are attractive due to their potential applications as hard coatings for cutting tools, turbine blades and machine components operating at high temperatures.

As a part of the 211 group of M<sub>n+1</sub>AX<sub>n</sub> phases, Cr<sub>2</sub>AlC was first reported by Jeitschko et al [1] and as a pure single-phase by other groups [3]. As determined in various other reports [4-7],

---

\*Corresponding author: ocrisan@yahoo.com

$\text{Cr}_2\text{AlC}$  has a hexagonal structure with  $P63/mmc$  space group, with the unit cell formed from two  $\text{Cr}_6\text{C}$  octahedra separated by a plane of Al atoms. Thin films of  $\text{Cr}_2\text{AlC}$  have reportedly been synthesized using magnetron sputtering techniques from elemental targets [4, 5] and from compound targets [6-9]. The method has been proven useful for other nanostructured materials as well [10-12]. In particular, using a dc magnetron sputtering from a compound target, Walter et al. [6] have reported formation of single-phase  $\text{Cr}_2\text{AlC}$  thin films on stainless steel substrates heated at temperatures lower than  $650^\circ\text{C}$ . In the present work, we report the deposition by sputtering onto Si(100) at  $200^\circ\text{C}$  of large area homogeneous thermal barrier coatings of  $\text{Cr}_2\text{AlC}$  followed by in-air and high-vacuum annealing as well as structural characterization of the resulting films.

## 2. Experimental

The DC sputtering facility used for deposition consists of a high vacuum chamber (initial pressure  $7 \times 10^{-7}$  mbar). DC sputtering was performed with 3 DC power sputtering sources. The sputtering targets were made of elemental Cr, Al and Carbon. The power of each source is tuneable such as to achieve the desired chemical composition. The thin films were deposited onto a Si (100) substrate in an Ar pressure of  $6.5 \times 10^{-4}$  mbar in the chamber. The substrate was heated to  $250^\circ\text{C}$  during 3 hours deposition. Film thickness was measured from the film cross-section by scanning electron microscopy (SEM) and found to be about  $1.2 \mu\text{m}$ .

Post-deposition annealing treatments have been performed in two ways:

- in a temperature-controlled oven in atmospheric conditions;
- in the high vacuum chamber using a temperature-controlled oven.

Samples were annealed at  $650^\circ\text{C}$  and  $700^\circ\text{C}$  for 30 min. While no special precautions were taken for the sample annealed in-air, for the high vacuum annealed samples, prior to the high temperature annealing, the sample was carefully outgassed by heating at intermediate temperatures of  $250^\circ\text{C}$  for 30 minutes.

The structure was investigated using grazing incidence X-ray diffraction (GIXRD). A Bruker Advanced D8 diffractometer with Cu  $K\alpha$  radiation was used for the XRD studies, while SEM images and EDX profiles were obtained using a field emission FEI microscope. Raman spectra were collected in the backscattering configuration using a Horiba Jobin Yvon spectrometer with CCD array detector. The light from Ar laser ( $514 \text{ nm}$ ) with a power of  $\sim 1.45 \text{ mW}$  was projected onto a spot size of  $\sim 2.5 \mu\text{m}$ . Nanoindentation of the film surface, performed using a nanoindenter from Keysight Technologies, with a Berkovich tip up to a maximum load of  $65 \mu\text{N}$ , provided elastic properties such as hardness and elastic bulk modulus.

## 3. Results and discussion

The as-deposited film is uniform, homogeneous and relatively flat as shown in the cross section SEM images in Fig. 1. The EDX measurements show that the Cr:Al:C relative composition is 50:25:25 ( $\pm 1$ ) at.%, close to the stoichiometry of  $\text{Cr}_2\text{AlC}$ .

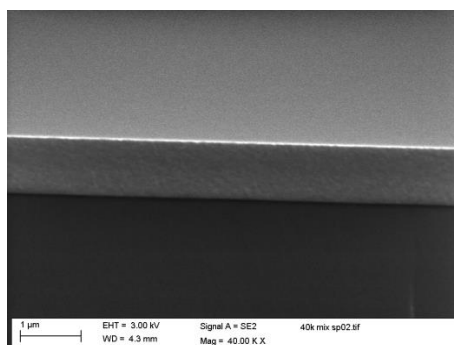


Fig. 1. Cross-section SEM image of the surface of the as-deposited  $\text{Cr}_2\text{AlC}$  thin film

### 3.1. In-air crystallization

The XRD pattern of the in-air annealed sample is presented in Fig. 2 together with the patterns for as-deposited and high vacuum annealed samples at 650°C and 700°C for 30 min, respectively. The grazing incidence  $2\Theta$  geometry was chosen for the XRD analysis in order to minimize the strong signals arising from the Si(100) Bragg lines. An incident angle of the X-ray beam of  $1.5^\circ$  ensured that there is minimal diffracted signal arising from the substrate itself.

The XRD pattern of the sample annealed in-air at 700°C for 30 min presents very sharp, well-defined Bragg lines (indexed by the corresponding  $(hkl)$  plane in Fig. 2) that are mostly attributed to the  $\text{Cr}_2\text{AlC}$  hexagonal structure ( $P63/mmm$  space group). Some other small peaks, probably belonging to oxides were observed.

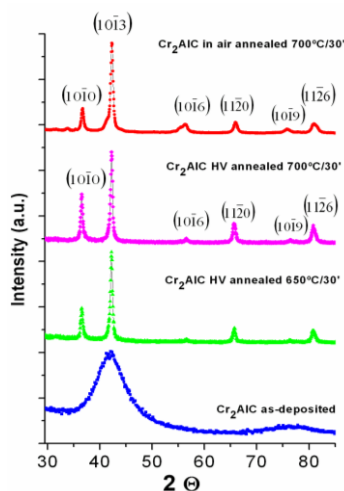


Fig. 2. XRD patterns of the samples from bottom to top: (i) as-deposited, (ii) high vacuum annealed at 650°C for 30 min, (iii) high vacuum annealed at 700°C for 30 min, (iv) in-air annealed at 700°C for 30 min

We have applied full-profile Rietveld-type refinement procedure on the XRD patterns, using Datlab software [13] in order to obtain the phase composition as well as structural parameters such as: lattice parameters and unit cell volume. We have also determined the average grain sizes and lattice microstrains using the integral breadth method [18-21].

The refinement procedure implies fitting of the Bragg peaks of the diagrams to a Voigt or pseudo-Voigt line profile. Such profile accounts for the physical broadening of XRD peaks by two mechanisms. The first one is strain-related and would produce a Gaussian profile, and the other is size-related and would produce a Lorentzian profile. The Voigt profile is thus a convolution of a Lorentz and a Gauss profile. The quantitative estimation of the Lorentz relative proportion in the Voigt profile is given by the mixing parameter which results from the fit.

The integral breadth method [14-17] calculates, using the lattice parameters, line widths and mixing parameters of each Bragg reflection, the average crystallographic domain size associated with the average size of the grains and the root mean square lattice microstrain. Here, the lattice microstrain is defined as the amount (change in size or volume) by which a crystal lattice deforms under stress or force and it is given as a ratio of the deformation to the initial lattice size, being a non-dimensional parameter.

In sputtered films stress is expected to be induced during deposition and, consequently, the lattice microstrains between the atomic planes could be significant. As one important issue that impedes the use of the thermal barrier coatings in industrial high temperature applications is represented by the deterioration of the coating by cracks and delamination, an understanding of the mechanisms that leads to accumulation of stresses in the structure and investigations of lattice microstrain could be essential.

For the in-air annealed sample, the hexagonal  $\text{Cr}_2\text{AlC}$  is found to be the main phase observed (94% of the total intensity of the Bragg reflections). Other small peaks have been identified as belonging to the rhombohedral  $\text{Cr}_2\text{O}_3$  structure ( $R\bar{3}c$  space group) with the total amount of 6%. This finding is in qualitative agreement with the WDSX analysis where we have determined that the oxygen is contained in 8% of the whole film thickness.

For the main  $\text{Cr}_2\text{AlC}$  hexagonal structure, lattice parameters close to those of the bulk phase are found from full-profile refinement analysis. An average grain size of around 32 nm and lattice microstrain of 0.24 has been determined using the integral breadth method. All parameters are depicted in Table 1.

Table 1: Lattice parameters, average crystal size and microstrain for the investigated samples

Sample	Lattice parameters			Crystal size (nm)	Microstrain (%)
	a (Å)	c (Å)	V (nm <sup>3</sup> )		
$\text{Cr}_2\text{AlC}$ – as-dep	2.87±0.07	13.16±0.04	0.281	8±3	0.81±0.06
$\text{Cr}_2\text{AlC}$ – HV 650°C	2.844±0.004	12.88±0.01	0.270	35±4	0.38±0.02
$\text{Cr}_2\text{AlC}$ – HV 700°C	2.837±0.003	12.85±0.02	0.267	39±3	0.25±0.02
$\text{Cr}_2\text{AlC}$ - in-air 700°C	2.849±0.009	13.18±0.04	0.278	32±4	0.24±0.03

The presence of the  $\text{Cr}_2\text{O}_3$  in the in-air annealed sample can be seen in the Raman spectrum (Fig. 3). The observed peaks were fitted using Lorentzian lines and peak positions are depicted in Table 2.

Table 2. Peak positions for as-deposited and annealed samples and corresponding literature values

Sample	Raman peak positions (cm <sup>-1</sup> )								
	1a	1b	1c	1d	2	3a	3b	4a	4b
$\text{Cr}_2\text{AlC}$ – as-dep	171	238	264	-	-	674	800	1372	-
$\text{Cr}_2\text{AlC}$ – HV 650°C	164	237	-	322	-	667	808	1375	1587
$\text{Cr}_2\text{AlC}$ – HV 700°C	167	236	-	326	-	672	807	1381	1592
$\text{Cr}_2\text{AlC}$ – in-air 700°C	167	252	305	343	552	694	792	1356	1560
Literature [18-22]	158	239	258	330	544	n/a	n/a	1350-1380	1550-1580

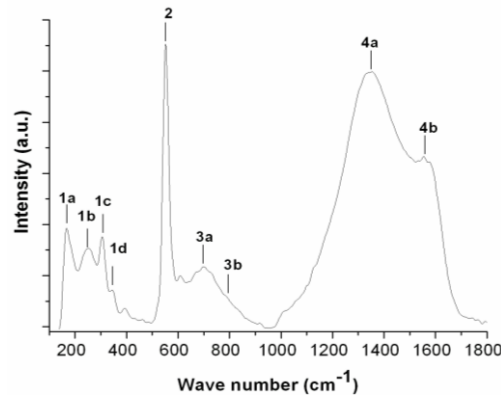


Fig. 3. Raman scan of the  $\text{Cr}_2\text{AlC}$  sample in-air annealed at 700°C for 30 min

The spectrum contains three important regions. The first region (between 120 and 400  $\text{cm}^{-1}$ ) presents peaks typical for  $\text{M}_2\text{AX}$  phases. As members of the space group  $\text{D}_{6h}^4$  the 211 structures of the larger class of MAX phases were reported to have 4 Raman-active optical modes, three of which are only Raman active ( $A_g+2E_{2g}$ ) and one is both Raman- and infrared-active ( $E_g$ ) [18]. 1a-1d peaks are attributed to these MAX phase modes. The assignment of the observed Raman peaks have been made in agreement with other reported results on  $\text{Cr}_2\text{AlC}$  [18,19].

The second region, between 550 and 900  $\text{cm}^{-1}$ , contains a very intense, strong peak assigned to  $\text{Cr}_2\text{O}_3$ , in agreement with Raman results on  $\text{Cr}_2\text{O}_3$  in [20]. Apart this sharp peak, two broad peaks, 3a-3b are observed. Since no other crystalline phase, other than the hexagonal  $\text{Cr}_2\text{AlC}$  and  $\text{Cr}_2\text{O}_3$ , is indexed in the XRD spectrum these peaks may possibly be attributed to other Raman active modes in the  $\text{Cr}_2\text{AlC}$  phase.

The third region, between 900 and 1800  $\text{cm}^{-1}$  shows the occurrence of very broad and intense Raman peaks, centred at about 1350 and 1550  $\text{cm}^{-1}$ . In agreement with various other reports [21,22] these peaks are attributed to the carbon D and G bands respectively. As the thin films of disordered carbon are often composed of covalent mixtures of  $\text{sp}^2$  - and  $\text{sp}^3$  -bonded carbon, Ferrari [21] assumed that the G peak is due to the bond stretching of all pairs of  $\text{sp}^2$  atoms while the D peak is due to the  $A_{1g}$  breathing modes and positions these peaks at 1360 and 1560  $\text{cm}^{-1}$ , respectively. Analysing Raman spectra of diamond-like-carbon thin films obtained by thermionic vacuum arc deposition, Musa et al [22] found very broad Raman peaks, similar to the peaks in Fig. 3, centred at around 1380 and 1560  $\text{cm}^{-1}$ , respectively, and attributed to the D and G carbon bands. In our case, it can be inferred that the development of the G-band signature indicates carbon nano-clustering upon annealing of the  $\text{Cr}_2\text{AlC}$  film. It is thought that this carbon can be partially responsible for the low friction coefficient of the  $\text{Cr}_2\text{AlC}$  phase.

### 3.2. High vacuum crystallization

The grazing incidence XRD measurements were also performed on the as-deposited  $\text{Cr}_2\text{AlC}$  and the samples high vacuum annealed at 650°C and 700°C. The XRD patterns of the samples are presented in Fig. 2. The spectra of the as-deposited film shows two broad lines centred at around 42° and 76° in  $2\theta$ . Such patterns are characteristic of a material structure made of small nanograins [23-25] with topological disorder [26,27] and amorphous-like structure [28]. The features are typical for short-range ordered materials and tend to suggest a solid solution of Cr-C [29]. After annealing in high vacuum at 650°C for 30 minutes, the XRD diagram changes to a well-defined pattern with sharp Bragg peaks, having the most intense peak (at around 42°) emerging from the narrowing of the broad line observed in the as-deposited case. The annealing at 650°C provides thus full crystallization of the film. The sample annealed at 700°C is characterised by slightly narrower peaks as compared to the case of 650°C annealing. Contrary to the case of in-air annealing, no detectable oxides or other phases in the 1% estimated errors range are observed in XRD patterns of the crystallized samples.

The diffraction patterns have been fitted using full-profile analysis [13,14]. As mentioned before, all the lines were indexed to the hexagonal  $\text{Cr}_2\text{AlC}$  phase, space group  $P63/mmc$ . The quantitative analysis did not show the presence of oxides or other phases. As previously mentioned, from the angular position, linewidth and mixing parameter of each pseudo-Voigt Bragg peak profile, we have derived the lattice parameters, calculated the unit cell volume and determined, using the integral breadth method [14-17], the average crystallographic domain size, assimilated to the average crystal size, as well as the lattice microstrain.

In Table 1, all the lattice parameters, unit cell volume, average crystal size and lattice microstrains for the three samples, as-deposited and high vacuum annealed at 650°C and 700°C are given.

It can be seen that while  $a$  decreases slightly with increasing temperature, the  $c$  parameter shows a more pronounced (3%) decrease for the sample annealed at 700°C than the as-deposited one. Usually in intermetallic alloys the re-crystallization occurs in two steps: primary and secondary crystallization, in nucleation and growth modes with different activation rates. In our case, during the re-crystallization process, higher crystallographic ordering occurs along the  $c$ -axes with formation of  $\text{Cr}_6\text{C}$  octahedral building blocks alternating with Al layers to form the  $\text{Cr}_2\text{AlC}$  nanolaminate structure [3]. The unit cell volume follows also a significant decrease upon

annealing the samples. In addition to crystallization, higher temperature annealing cause the  $\text{Cr}_2\text{AlC}$  hexagonal lattice to exhibit lesser defects, therefore diminishing the average unit cell volume.

As a result of the crystallization process the average grain size increases from 8 nm, for the as-deposited sample, to around 35 and 39 nm in the case of the samples annealed at 650°C and 700°C. It is interesting to note that, upon annealing, the lattice microstrain decreases by almost 70% compared to the as-deposited case.

An interesting aspect is observable if one compares the lattice parameters in the two samples annealed in-air and under high vacuum at 700°C. For same annealing temperature, the lattice parameters, especially the  $c$  parameter, as well as the unit cell volume are higher for the in-air annealed sample than for the high-vacuum annealed sample. This means that the hexagonal lattice is expanded along the  $c$ -axis. As the  $c$ -axis is the direction along which the stacking of the octahedral  $\text{Cr}_6\text{C}$  building blocks alternate with Al atomic layers, it follows that, during in-air crystallization, more defects, most probably oxygen atoms, are incorporated into the lattice. These defects are related to the presence of oxygen. While part of the oxygen is located in the  $\text{Cr}_2\text{O}_3$  phase formed at the surface of the coating, some of the oxygen atoms may also be incorporated into the hexagonal  $\text{Cr}_2\text{AlC}$  lattice giving rise to a larger unit cell, elongated along the stacking direction, for the in-air annealed sample compared to the high vacuum annealed sample

The as-deposited and high-vacuum annealed  $\text{Cr}_2\text{AlC}$  thin films have been also analyzed using Raman spectroscopy in the same conditions as for the in-air annealed sample. All scans are presented in Fig. 4. As in the other case, three typical areas can be separated. The first area (between 120 and 400  $\text{cm}^{-1}$ ) presents the 1a-1d peaks typical for 211 phases. While in the as-deposited sample, the  $\text{Cr}_2\text{AlC}$ -related peaks are very broad and overlap, the crystallized samples show three sharp, well-defined peaks. Also, in the case of the as-deposited sample, the positions of the broad peaks are shifted compared with their crystalline counterparts. No significant peak position displacement is observed between the samples high-vacuum annealed at 650°C and those annealed at 700°C.

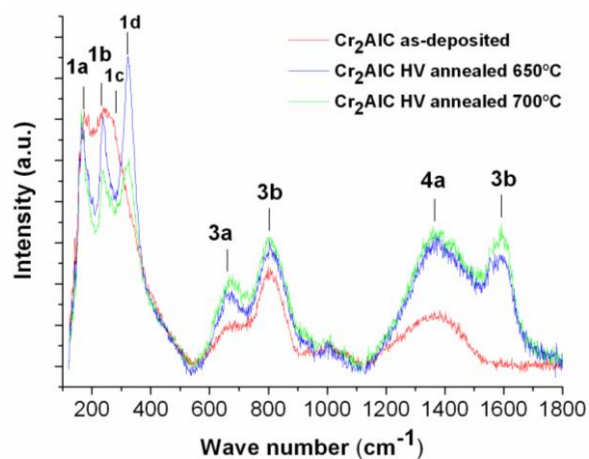


Fig. 4. Raman spectra for  $\text{Cr}_2\text{AlC}$  as-deposited and high-vacuum annealed samples

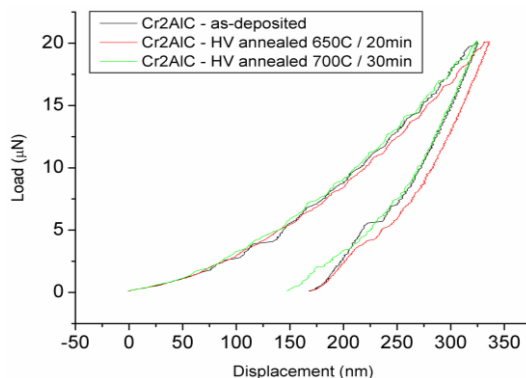


Fig. 5. Typical load-displacement curves obtained by nanoindentation of  $\text{Cr}_2\text{AlC}$  as-deposited and high-vacuum annealed samples

While the 1a peak has almost the same value as for the in-air annealed sample, the 1b, 1c and 1d Raman peaks are observed at lower wavenumbers, for as-deposited and high-vacuum annealed samples, than those of the in-air annealed samples, and show better agreement with previously reported results [18,19]. In the as-deposited case, the 1b and 1c peaks are overlapping while the 1d ( $A_g$ ) peak is not observed until after full crystallization. On the contrary, in the fully crystallized samples, the 1c ( $E_{2g}$ ) cannot be seen in the experimental spectra.

Upon crystallization, the 1a, 1b and 1d peaks are better resolved and sharper than in the case of the as-deposited sample. The peak sharpening after annealing can be explained on the basis of phonon confinement [30]. The sharpening of the relevant Raman peaks upon annealing confirms the XRD findings where we have observed full crystallization and formation of  $\text{Cr}_2\text{AlC}$  upon annealing at 650°C. By comparison with Fig. 3, the vacuum-annealed samples show more intense and better resolved peaks, nevertheless unlike the in-air annealed case, in the high-vacuum annealed samples, the 1c peak is not observed.

The second region, between 550 and 900  $\text{cm}^{-1}$ , does not now show the  $\text{Cr}_2\text{O}_3$  Raman peak for the as-deposited and high-vacuum-annealed samples, as was expected and confirmed by the XRD and WDX results where no measurable oxides were observed for the as-deposited and high-vacuum annealed samples. The 3a and 3b peaks are more visible and better formed for the high-vacuum annealed samples. Since XRD results show single phase  $\text{Cr}_2\text{AlC}$  for the high-vacuum annealed samples, we assume, as in the case of the in-air annealed samples, that these two peaks belong to Raman modes of the MAX phase.

In the third region, between 1100 and 1800  $\text{cm}^{-1}$  as in the case of in-air annealed sample, the 4a and 4b Raman peaks assigned to the D and G band of carbon are observable for the as-deposited and high-vacuum annealed samples. While in the as-deposited sample, only the D band is observable, for the high vacuum annealed samples, a sharper, relatively intense peak assigned to the carbon G band is observed. It has been reported that the D mode of carbon originates from a double-resonance Raman scattering process [31,32]. In this process, the incident photon resonantly excites an electron-hole pair. The electron is subsequently scattered under emission/absorption of a phonon. To satisfy momentum conservation, the electron has to be scattered back to a point in k-space where its momentum is near that of the initial hole [33]. For the D mode in the Raman spectrum, the backscattering is achieved by a defect in the graphite lattice. Therefore, as perfect graphite is assumed to show no D band, it is considered as being a “disorder-induced” band of carbon [34]. From this point of view, its detection in the as-deposited Raman spectrum is a confirmation of the XRD results that showed an amorphous-like structure of the as-deposited sample. The G band intensity is assumed not to be dependent on defects therefore the presence of a narrower G band in the Raman spectra infers a certain degree of ordering and carbon clustering.

The possibility of this nanoclustering of carbon in the  $\text{Cr}_2\text{AlC}$  films needs further discussion. Studying the effect of the composition on the structure of Cr-Al-C, Mertens et al. [5] correctly pointed out that, while deviations from stoichiometry in MAX phases have been experimentally observed, XRD patterns did not indicate the presence of a second phase. According

to the ternary phase diagrams, deviations from stoichiometry should result in formation of supplemental binary phases. Based on XRD results and *ab-initio* calculations, they conclude that deviations from stoichiometry of up to 6.3 at% Al, (or Cr/C ratio between 1.72 and 1.93, Cr/Al ratio between 1.42 and 2.03) still result in occurrence of only a single Cr<sub>2</sub>AlC phase, in the XRD patterns. Possible pathways for accommodating these deviations were presented by Mertens et al. [5] under a model that explains these extended compositional ranges by “segregation of material which escapes detection by XRD, segregation of an amorphous phase or another phase that cannot be detected by XRD”. They calculate by *ab-initio* VASP code, various structures including, perfect Cr<sub>2</sub>AlC, stacking fault hexagonal structure with Al excess, and structures obtained by interstitial Al substitutions. As previously mentioned, compared with Mertens results, our values for the lattice parameters and unit cell volume for fully crystallized samples 1a and 2a, fit within the model of a Cr<sub>2</sub>Al<sub>1.1</sub>C hexagonal structure with stacking faults. Taking into account the composition we have determined for our sample, the excess of Al in our structure may be explained, based on Mertens arguments, by the segregation of material that escapes detection in XRD. This material is carbon, as we have observed the pronounced G-band of carbon in the Raman spectra of fully crystallized samples, assimilated to the carbon nanoclustering during annealing. This represents a confirmation of Mertens model, and explains the occurrence of free carbon, not detected by XRD, by the Al excess in the Cr<sub>2</sub>AlC stacking faults structure. It is proven thus, that high-vacuum annealing of the Cr<sub>2</sub>AlC thin films leads to ordering and the formation of carbon nanoclusters within the film.

### 3.3. Elastic properties

In order to estimate some of the elastic properties of our samples, we have performed nanoindentation experiments using a Keysight technologies device with Berkovich tip. Load-displacement curves have been obtained on the as-deposited and high vacuum annealed annealed at 650° and 700°C samples. Representative load-displacement curves for the 20 μN load are depicted in Fig. 6 and results for the hardness *H* and elastic reduced modulus *Er* are schematically presented in Table 3. It can be seen that, whereas a small increase of the hardness is observed in annealed samples compared with as-deposited one, this increase is within the experimental errors. Hardness values for our Cr<sub>2</sub>AlC samples are between 12.5 and 12.8 GPa while elastic modulus, calculated from reduced bulk modulus via the proportionality constant  $3(1-2\nu)=1.584$  [35], ranges between 241 and 247 GPa. These results are consistent with previously reported values. For comparison, hardness and elastic modulus reported in [35] for Cr<sub>2</sub>AlC thin films are 13.5 GPa and 298 GPa. Hardness values for thin films are significantly larger than those of bulk MAX phases, in general. In the case of Cr<sub>2</sub>AlC bulk material, this value does not generally exceed 3.5 GPa [36]. This difference is explained [35] by the reduction of grain size towards the scale of few tens of nanometers and increase of the density of grain boundaries in thin films, comparing with the bulk materials where the grains have sizes typically in the micrometer range [37-44]. This interpretation explains also the high hardness value obtained for the amorphous-like as-deposited film, compared with annealed, nanocrystallized films. Whereas as-deposited samples do not exhibit hexagonal crystal structure, the average grain size is of the order of few nanometers, as determined from XRD studies. This is consistent with the enhanced value of hardness, comparable with those of crystallized thin films.

Table 3. Hardness, reduced bulk and elastic moduli obtained after nanoindentation with 20 μN load for as-deposited and annealed samples and some representative literature values

Sample	Elastic properties		
	Hardness H (GPa)	Reduced modulus (GPa)	Elastic modulus(GPa)
Cr <sub>2</sub> AlC – as-dep	12.57±0.3	152±3	241±5
Cr <sub>2</sub> AlC – HV 650°C	12.64±0.6	155±4	245±6
Cr <sub>2</sub> AlC – HV 700°C	12.77±0.7	156±4	247±6
Literature [36]	13±2	-	298±21

#### 4. Conclusions

The ternary alloys of composition  $\text{Cr}_2\text{AlC}$  belonging to the larger class of MAX-phases were deposited by DC sputtering onto Si(100) substrates at 200°C. The material was subsequently annealed in-air at 700°C and also high vacuum annealed at 650°C and 700°C for 30 min. As-deposited and annealed films are shown to be homogeneous and dense over large areas. XRD analysis shows the formation of an amorphous-like Cr-C-Al solid solution in the as-deposited state. In-air annealing at 700°C produces complete re-crystallization of the sample. Full-profile fitting of the XRD pattern of in-air annealed samples reveals that main phase identified is hexagonal  $\text{Cr}_2\text{AlC}$  (94%). The rhombohedral  $\text{Cr}_2\text{O}_3$  phase is also identified in the XRD pattern. When annealed in high vacuum, the samples become fully crystallized upon annealing at 650°C and have a single-phase  $\text{Cr}_2\text{AlC}$  hexagonal structure, as proven by full-profile XRD pattern analysis. Lattice parameters and unit cell volume are shown to decrease upon annealing due to grain growth during re-crystallization accompanied by a relaxation of lattice defects. The grain size has been calculated using an integral breadth approach from the XRD patterns and shown to increase upon annealing. Lattice microstrain is shown to drastically decrease to almost 70% in the coating upon annealing, thereby providing an extra means of controlling improvement of the desired mechanical properties of these coatings. Raman spectra exhibit peaks (1a-1d) assigned to  $\text{Cr}_2\text{AlC}$  in agreement with previous reports and we identified also supplemental peaks (3a-3b) attributed to other Raman-active modes in the  $\text{Cr}_2\text{AlC}$  phase. The peaks are narrower and better defined for re-crystallized samples compared to as-deposited films. Although the D band of carbon is observed in the as-deposited sample, a narrow, intense and well-defined Raman peak attributed to the G band appears in the annealed samples indicating an enhanced degree of ordering and possible nano-clustering of carbon upon annealing the  $\text{Cr}_2\text{AlC}$  thin films. Hardness values of about 12-13 GPa are obtained from nanoindentation measurements, for both as-deposited and annealed samples. Such values, significantly larger than those of bulk materials, may be explained by the drastic decrease of the average grain size, towards few nanometers and increase of the density of grain boundaries.

#### Acknowledgements

The financial support of the Romanian Ministry of Research and Innovation via PN-III-P4-ID-PCE-2016-0833 is gratefully acknowledged.

#### References

- [1] W. Jeitschko, H. Nowotny, A. Benesovsky, *Monash. Chem.* **94**, 672 (1963).
- [2] M.W. Barsoum and T. El-Raghy, *Amer. Sci.* **89**, 334 (2001).
- [3] P. Eklund, M. Beckers, U. Jansson, H. Hogberg and L. Hultman, *Thin Solid Films* **518**, 1851 (2009).
- [4] J.M. Schneider, Z. Sun, R. Mertens, F. Uestel and R. Ahuja, *Solid State Commun.* **130**, 445 (2004).
- [5] R. Mertens, Z. Sun, D. Music and J.M. Schneider, *Adv. Eng. Mater.* **6**, 903 (2004).
- [6] C. Walter, D.P. Sigumonrong, T. El-Raghy and J.M. Schneider, *Thin Solid Films* **515**, 389 (2006).
- [7] D.V. Shtansky, P.V. Kiryukhantsev-Korneev, A.N. Sheveyko, B.N. Mavrin, C. Rojas, A. Fernandez and E.A. Levashov, *Surf. Coat. Technol.* **203**, 3595 (2009).
- [8] J.J. Li, L.F. Hu, F.Z. Li, M.S. Li and Y.C. Zhou, *Surf. Coat. Technol.* **204**, 3838 (2010).
- [9] Q.M. Wang, A. Flores Renteria, O. Schroeter, R. Mykhaylonka, C. Leyens, W. Garkas, M. to Baben, *Surf. Coat. Technol.* **204**, 2343 (2010).
- [10] O. Crisan, A.D. Crisan, *J. Alloys & Compd.* **509**, 6522 (2011).
- [11] O. Crisan, A.D. Crisan, N. Randrianantoandro, R. Nicula, E. Burkel, *J. Alloys & Compd.* **440**, L3-L7 (2007).

- [12] O. Crisan, J.M. Le Breton, M. Nogues, F. Machizaud, G. Filoti, *J. Phys: Condens. Matter* **14**, 12599 (2002).
- [13] K. Syassen, Datlab, version 1.38XP MPI/FKF Stuttgart, Germany, (2005).
- [14] H.P. Klug and L.E. Alexander, "X-ray Diffraction Procedures 2<sup>nd</sup> edition John Wiley", New York, (1974).
- [15] D. Balzar and H. Ledbetter, *J. Appl. Cryst.* **26**, 97 (1993).
- [16] D. Balzar, *J. Res. Natl. Inst. Stand. Technol.* **98**, 321 (1993).
- [17] B.E. Warren, "X-ray Diffraction, Addison Wesley", Reading, MA, (1969).
- [18] J.E. Spanier, S. Gupta, M. Amer and M.W. Barsoum, *Phys. Rev. B* **71**, 012103 (2005).
- [19] O.D. Leaffer, S. Gupta, M.W. Barsoum and J.E. Spanier, *J. Mater. Res.* **22**, 2651 (2007).
- [20] J. Kajikawa, *J. Cryst. Growth* **289**, 387 (2006).
- [21] A.C. Ferrari, *Solid State Commun.* **143**, 47 (2007).
- [22] G. Musa, R. Vladoiu, V. Ciupina, J. Janik, *J. Optoelectron. Adv. Mat.* **8**, 621 (2006).
- [23] M. Seqqat, M. Nogues, O. Crisan, *J. Magn. Magn. Mater.* **157**, 225 (1996).
- [24] O. Crisan, K. von Haefen, A.M. Ellis, C. Binns, *J. Nanopart. Res.* **10** (suppl.1), 193 (2008).
- [25] O. Crisan, M. Angelakeris and N.K. Flevaris, *J. Optoelectron. Adv. Mat.* **5**, 959 (2003).
- [26] O. Crisan, J.M. Le Breton and G. Filoti, *Sensors & Actuators A* **106**, 246 (2003).
- [27] O. Crisan, Y. Labaye, L. Berger, J.M. Greneche and J.M.D. Coey, *J. Appl. Phys.* **91**, 8727 (2002).
- [28] O. Crisan, J.M. Greneche and J.M. Le Breton, *Eur. Phys. J. B* **34**, 155 (2003).
- [29] J. Högström, M. Hanson, S. Urbonaite, A. Furlan, W. Fredriksson, K. Edström, U. Jansson, L. Nyholm, Abstract 1220, 218<sup>th</sup> Electrochemical Society (ECS) Meeting, Las Vegas, (2010).
- [30] I.H. Campbell, P.M. Fauchet, *Solid State Commun.* **58**, 739 (1986).
- [31] C. Thomsen, S. Reich, *Phys. Rev. Lett.* **85**, 5214 (2000).
- [32] J. Maultzsch, S. Reich, C. Thomsen, *Phys. Rev. B* **64**, 121407(R) (2001).
- [33] M. Kalbac, Y.P. Hsieh, H. Farhat, L. Kavan, M. Hofmann, J. Kong, M.S. Dresselhaus, *Nano Lett.* **10**, 4619 (2010).
- [34] M.S. Dresselhaus, A. Jorio, and R. Saito, *Annu. Rev. Cond. Matter Phys.* **1**, 89 (2010).
- [35] J.M. Schneider, D.P. Sigumonrong, D. Music, C. Walter, J. Emmerlich, R. Iskandar, J. Mayer, *Scripta Mater.* **57**, 1137 (2007)
- [36] W. Tian, P. Wang, G. Zhang, Y. Kan, Y. Li, D. Yan, *Scripta Mater.* **54**, 841 (2006).
- [37] M. Sofronie, F. Tolea, V. Kuncser, *J. Appl. Phys.* **107**, 113905 (2010).
- [38] F. Tolea, M. Tolea, M. Sofronie, *Solid State Commun.* **213**, 37 (2015).
- [39] F. Tolea, M. Sofronie, C. Ghica, *Optoelectron. Adv. Mater. – Rapid Commun.* **5**, 562 (2011).
- [40] M. Rosenberg, V. Kuncser, O. Crisan, *J. Magn. Magn. Mater.* **177**, 135 (1998).
- [41] M. Sofronie, F. Tolea, V. Kuncser, *IEEE Trans. Magn.* **51**, 2500404 (2015).
- [42] V.R. Reddy, O. Crisan, A. Gupta, V. Kuncser, *Thin Solid Films* **520**, 2184 (2012).
- [43] F. Tolea, M. Sofronie, M. Tolea, *Dig. J. Nanomater. Biostruct.* **10**, 567 (2015).
- [44] A.D. Crisan, R. Nicula, O. Crisan, *Mater. Sci. Eng. C – Biomimetic Supramol. Syst.* **27**, 1280 (2007)